Fluids and Barriers of the CNS

RESEARCH

Open Access

Blood-CSF barrier clearance of ABC transporter substrates is suppressed by interleukin-6 in lupus choroid plexus spheroids

Joshua A. Reynolds[1], Lola Torz[2,3], Leslie Cummins[4], Ariel D Stock[5], Ayal Ben-Zvi[6] and Chaim Putterman[7,8*]

Abstract

Background The choroid plexus (CP) has been recently implicated in the pathogenesis of the neuropsychiatric manifestations of systemic lupus erythematosus (NPSLE). Lupus patients demonstrate increased serum and cerebrospinal fluid (CSF) concentrations of interleukin-6 (IL-6), which can disrupt vital blood-CSF barrier (B-CSFB) functions performed by the CP. However, difficulty accessing this tissue has largely precluded dynamic imaging or evaluation of CP barrier function in vivo.

Methods In this study, explant CP spheroids which replicate the functional and structural properties of the B-CSFB were generated from 12 + week old female MRL/lpr (IL-6 wildtype; IL-6 WT) lupus mice, IL-6 knockout (IL-6 KO) MRL/lpr mice, and congenic control MRL/mpj mice. CP spheroids derived from IL-6 WT MRL/lpr mice were found to synthesize and secrete IL-6, similar to the CP in vivo, whereas the IL-6 KO spheroids did not produce IL-6. Accumulation of different fluorescent tracers within the central CSF-like fluid vacuole of spheroids, modeling brain ventricles, was measured to probe transcellular permeability, paracellular diffusion, and clearance functions of the CP.

Results As shown by blocking the IL-6 receptor in IL-6 WT spheroids or comparing them to IL-6 KO spheroids, IL-6 signaling decreased spheroid clearance of methotrexate, a chemotherapeutic drug employed in the therapy of lupus, and lucifer yellow. This suppression occurred without altering CP epithelial morphology and ultrastructure. Methotrexate and lucifer yellow efflux can occur through ATP-binding cassette (ABC) transporters, including BCRP and MRP1. Cytoplasmic accumulation of the ABC-specific dye fluorescein diacetate was also increased by IL-6. Pharmacologic inhibition of either BCRP or MRP1 in IL-6 KO spheroids was sufficient to recreate the clearance deficits observed in IL-6 WT spheroids. Moreover, CP expression of BCRP was significantly lower in IL-6 WT mice.

Conclusions In this study, we establish, validate, and apply a CP spheroid model to the study of B-CSFB function in lupus. Our results show that IL-6, a key cytokine increased in NPSLE, can potentially suppress the CP-specific function and expression of BCRP and MRP1. Therefore, IL-6 could affect the CSF clearance of inflammatory substrates (e.g., leukotrienes), the accumulation of which would incite neurotoxicity and promote progression of NPSLE.

*Correspondence:
Chaim Putterman
chaim.putterman@einsteinmed.edu

Full list of author information is available at the end of the article

Keywords NPSLE, Cerebrospinal fluid, blood-CSF barrier, Interleukin-6, BCRP, MRP1

Background

A debilitating multisystem inflammatory disease, systemic lupus erythematosus (SLE) primarily affects women between the ages of 15 and 45 [1, 2]. Among its many manifestations, neuropsychiatric involvement, or neuropsychiatric lupus (NPSLE), worsens the prognosis of lupus patients [3]. 50% or more of lupus patients experience neurologic symptoms during their lifetime [4]. A subset of these sequelae can be attributed to cerebrovascular disease secondary to hypercoagulability caused by autoantibodies that target phospholipids [5]. Symptoms without a defined etiology, termed diffuse NPSLE, include cognitive dysfunction, memory loss, mood disorder, and anxiety [6]. Clear signs of neuronal pathology are often found in patients with diffuse NPSLE. Cortical atrophy and diffuse white matter abnormalities correspond with cognitive symptoms in imaging studies [7, 8]. A neuroinflammatory process is further evidenced by the elevated cerebrospinal fluid (CSF) levels of autoantibodies and cytokines in NPSLE patients [9, 10].

Disruption of the blood-CSF barrier could promote a neuroinflammatory environment within the CSF and in turn promote neurotoxicity. Located within the brain's ventricular system, the choroid plexus (CP) comprises this vital barrier [11]. Cuboidal epithelial cells arranged in a continuous single layer envelop fenestrated capillaries and other stromal cells [12]. Able to freely sample the serum via these fenestrations, the CP epithelia filter which blood products enter the ventricles to produce the CSF by first establishing minimally permeable paracellular tight-junctions and then selectively moving substrates through membrane channels, transporters, and vesicular trafficking [13, 14]. CP epithelia can also synthesize and secrete beneficial molecules like neurotrophic cytokines [13].

Equally as important as adding substrates, the CP also "sanitizes" the CSF of harmful molecules. This clearance function removes metabolic waste, excess neurotransmitters, inflammatory molecules, and other neurotoxins to ensure normal function of neuronal tissue [12, 13]. ATP-binding cassette (ABC) transporters are vitally important to epithelial clearance. Well known for their ability to efflux potentially harmful drugs, this class of membrane proteins also transports endogenous neurotoxic metabolites like porphyrins, uric acid, and leukotrienes. P-glycoprotein (P-gp), multi-drug resistance protein 1 (MRP1), and breast cancer resistance protein (BCRP) represent the most common ABC transporter subtypes in epithelial cells [15].

In NPSLE, there are pronounced signs of CP pathology. Peripheral immune cells including lymphocytes and macrophages infiltrate the CP in NPSLE patients and animal models. These immune aggregates, which form into tertiary lymphoid structures, can generate antibodies and secrete inflammatory cytokines [16, 17]. A recent clinical imaging study in human SLE found enlargement of the CP, a sign of neuroinflammation, which was even more pronounced in NPSLE patients [18]. Similar enlargement of the CP was recently described in non-lupus patients with major depressive disorder, and that enlargement appeared to be linked to serum levels of cytokines, including those of the interleukin family [19].

High interleukin-6 (IL-6) concentrations are found in the serum of NPSLE patients [9, 20]. Furthermore, among other soluble inflammatory mediators, IL-6 is the molecule most often elevated in NPSLE patients' CSF, and its presence there has been associated with neuropsychiatric involvement [21]. In response to inflammation, the CP cells upregulate IL-6 expression [22]. Whether from the serum, CSF, or epithelial cells themselves, the CP is therefore likely exposed to consistently high levels of IL-6 in NPSLE. Comparable inflammatory cytokines, including interferon-γ, have previously been shown to disrupt epithelial barriers elsewhere in the body [23, 24]. As evidenced by inflammatory changes in the CP tissue and CSF composition, blood-CSF barrier disruption appears likely in NPSLE. Specifically, IL-6 could promote dysfunction of this key barrier.

To evaluate this proposed model of disease, we investigated the integrity of the CP in the MRL/lpr mouse model of lupus and control MRL/mpj mice. This model develops many immunologic and organ-system correlates of human lupus pathology ("lupus-prone"), including elevated serum anti-double stranded DNA and other characteristic anti-nuclear autoantibodies, autoreactive T cells, dermatitis, arthritis, proliferative glomerulonephritis, neuroinflammation, memory deficits, and affective features. As a result of this high fidelity to human disease, the MRL/lpr strain is widely used to model NPSLE [25, 26]. We further studied changes to clearance functions of the CP in MRL/lpr mice lacking IL-6 expression. Several experimental complexities limit in vivo functional study of the CP. For example, its location deep within the ventricles makes direct observation challenging [12]. While intravital imaging of immune cell migration across the CP has recently been achieved by implanting large windows [27], assessment of CP epithelial cell permeability to small inflammatory molecules has yet to be achieved in vivo. Similarly, quantifying CSF contents falls short of discerning specific CP pathology as the fluid's composition receives contributions from brain tissue [13]. For these reasons, we resolved to study the lupus CP ex vivo.

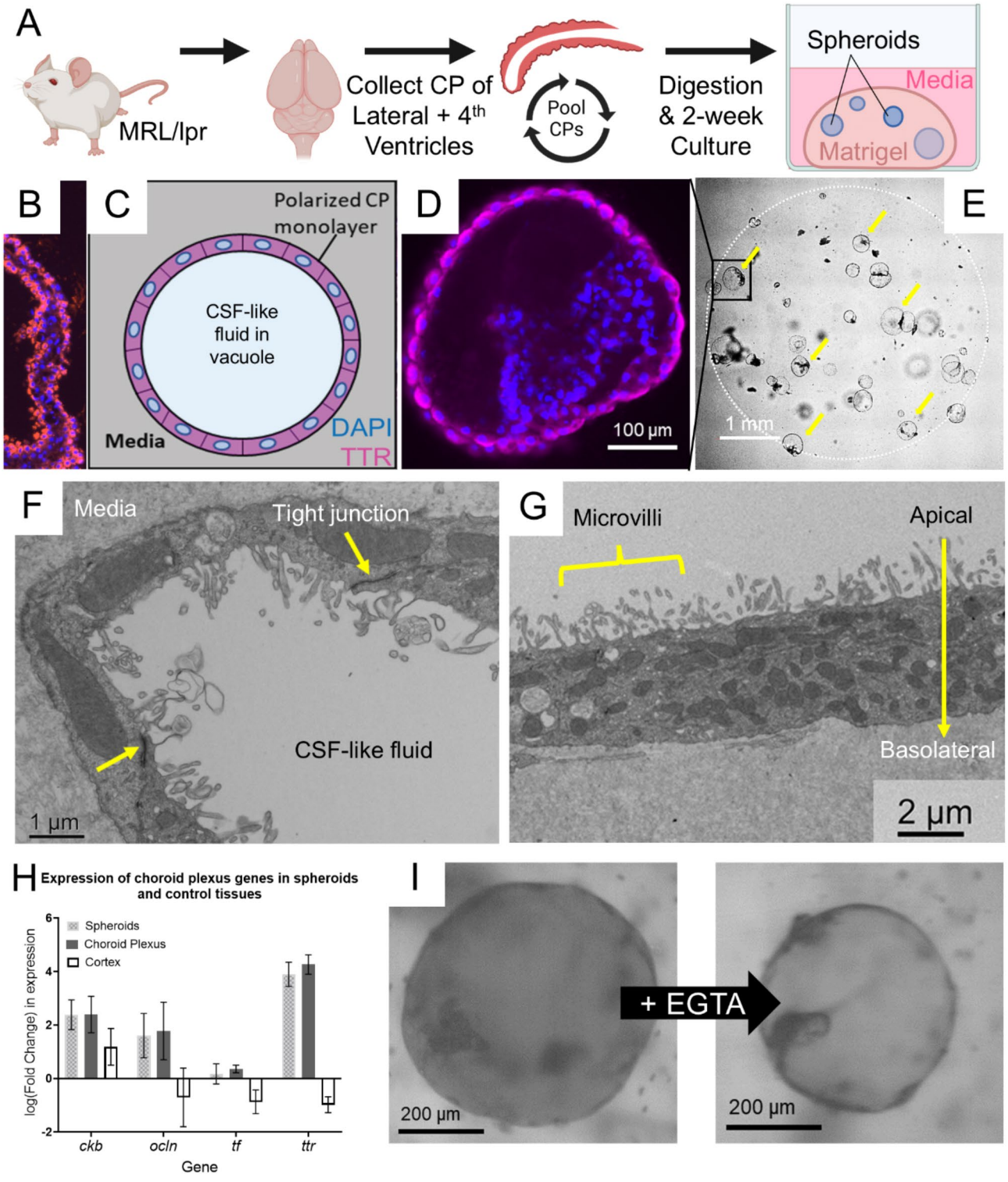

Fig. 1 (See legend on next page.)

While CP epithelial monolayers can be used to study barrier permeability, three-dimensional organoid and spheroid models provide much better replication of the CP's in vivo morphology [28].

Modifying a recently published protocol [29], we generated spheroids from primary CP cells explanted from adult lupus and control mice. Moreover, we generated spheroids from an IL-6 knockout MRL/lpr strain to test IL-6 specific effects on CP spheroid function. We

(See figure on previous page.)

Fig. 1 Validation of the choroid plexus spheroid model in lupus mice. Validation of the choroid plexus spheroid model in lupus mice. **(A)** The spheroid generation protocol [29] involved collection of brains from multiple mice followed by dissection to collect choroid plexus (CP) tissue from both lateral ventricles and the fourth ventricle. CP samples from multiple mice were pooled, then mechanically digested and washed. Explanted tissue was suspended in domes of synthetic extracellular matrix (Matrigel). Following two weeks in epithelia-selective media, many 3D spherical CP spheroids were present in each culture well. **(B)** In vivo CP of a mouse demonstrating the distribution of transthyretin (TTR; canonical CP marker; purple) in the epithelial cytoplasm. **(C)** Spheroid schematic depicting cross-section of expected spheroid morphology with continuous layer of polarized, TTR-expressing epithelial cells surrounding a central CSF-like fluid compartment. **(D)** Immunofluorescent whole mount image of an spheroid cross-section demonstrating TTR distribution similar to the CP in vivo. **(E)** A representative low-magnification image showing many spheroids (yellow arrows) per well. The dashed white circle indicates the boundary of the Matrigel dome. **F-G)** Representative high-magnification transmission electron microscopy images of CP spheroid epithelial cells confirming formation of a distinct fluid compartment. Inter-epithelial tight junctions appear intact. Apical and basolateral polarity is evident in microvilli formation on the CSF-facing side, as occurs in vivo. Apical to basolateral direction of clearance activity is indicated by the arrow (right). **H)** Real-time quantitative PCR was used to quantify gene expression in CP spheroids, in vivo CP (positive control), and in vivo cortex (negative control; *ckb*: brain creatine kinase; *ocln*: ocludin; *tf*: transferrin; *ttr*: transthyretin). **I)** Spheroid collapse caused by tight junction disruption indicates intact paracellular integrity (EGTA: egtazic acid, calcium chelation)

hypothesized that as compared to spheroids derived from the control MRL/mpj strain, MRL/lpr spheroids would exhibit abnormalities in transcellular permeability, paracellular diffusion, and clearance functions. We further hypothesized that IL-6 knockout MRL/lpr spheroids would demonstrate restored integrity of these pathways.

Methods

Animals

The experimental groups included MRL/lpr lupus prone mice and age-and-sex matched congenic control MRL/mpj mice. Additionally, *il6* -/- MRL/lpr (IL-6 KO) mice and *il6* +/+ homozygous MRL/lpr littermates (IL-6 WT) [30] were studied. IL-6 WT spheroids, rather than non-lupus MRL/mpj ones, served as the control group in studies of IL-6 effects, because an intact IL-6 gene is their defining genetic distinction from IL-6 KO spheroids. To generate CP spheroids from each genotype, the protocol used adult female mice of at least twelve weeks of age, the sex and age of MRL/lpr mice which display significant neuropsychiatric deficits [26, 31–33]. All animal husbandry and handling protocols were approved by the Institutional Animal Care and Use Committee at the Albert Einstein College of Medicine (AECOM; Bronx, NY). All mice were housed in a specific-pathogen free environment at AECOM.

Spheroid generation

Adapting a protocol in C57BL/6J mice published by Petersen et al. [29], we generated spheroids from primary CP cells explanted from the study mice. CP from lateral and 4th ventricles of multiple mice were pooled, mechanically dissociated, plated, and cultured for two weeks (Fig. 1A). Across all experiments, 118 explants were collected in total. Prepared explants were plated and cultured in Matrigel domes on an eight well chambered microscopy slide ("µ-slide") at a ratio of explants from two mice per four wells. Each well contained dozens of individual spheroids of the same genotype. The culture media contained pro-epithelial cytokines in DMEM and was changed regularly without passaging the spheroids onto new slides. Additional experimental detail and reagent information is provided in the Supplementary Materials and Methods.

Quantification of gene expression

Gene expression was measured using real-time quantitative polymerase chain reaction (qPCR) analysis following RNA isolation, cDNA synthesis, qPCR, and analysis protocols previously published [29, 34]. To collect sufficient high-quality RNA, several wells of spheroids were pooled separately for each genotype. Gene expression within five spheroid pools was compared to five pools of ex vivo tissue aliquoted from the same mice. CP samples used for the in vivo ABC transporter expression assays were collected from sixteen-week-old female IL-6 KO and IL-6 WT mice.

Immunofluorescent staining

Brains were collected, paraffin-embedded, sectioned, stained, and imaged as previously described [34]. In one experiment, immunofluorescent labelling was performed which identified the canonical CP marker [35] transthyretin (TTR; chicken-anti-mouse TTR primary antibody; Invitrogen, Waltham, MA; Cat# PA5-20742; 1:100) in brain sections from an MRL/lpr mouse. Separately, the ABC transporter BCRP (rabbit-anti-mouse BCRP primary antibody; Sigma, St. Louis, MO; Cat#ZRB1217; 1:200) was labelled in brain sections from eight IL-6 WT and eight IL-6 KO mice. In both experiments, nuclei were stained using DAPI. Similarly, whole mount immunofluorescent labeling of TTR was performed in spheroids as described previously [36], and images were collected using a Nikon CSU-W1 spinning disk confocal microscope. Image processing used NIS-Elements (Nikon) and ImageJ [37] software. Qualitative assessment of BCRP fluorescence was performed blindly on unaltered images, scaled from 1 (minimal) to 4 (marked).

Spheroid electron microscopy

Spheroids of a single genotype were cultured in single-well glass bottom 35 mm dishes to facilitate preparation

for electron microscopy [16]. Images were collected using a JEOL 1400 Plus transmission electron microscope. Three spheroids per genotype (IL-6 WT, IL-6 KO, or MRL/mpj) were imaged and blindly evaluated by an experienced electron microscopist (L.C.) for positioning of epithelial cells, tight junction integrity, mitochondria, nuclear integrity and chromatin state, endocytic pit formation, microvilli, and ciliation. In addition to these qualitative comparisons, microvilli coverage (defined as the percent of spheroid circumference covered by microvilli) and tight junction number (defined as the number of tight junctions per millimeter of circumference) were quantified for each spheroid and compared between genotypes.

IL-6 protein quantification

We measured IL-6 concentrations in the media of 2–4 wells of mature spheroids per each genotype using the mouse IL-6 Quantikine ELISA kit (R&D Systems). All values were normalized to a sample of fresh media (no spheroid blank). A standard curve was generated, from which concentrations of each sample were calculated.

Tracer studies: CSF-like vacuole accumulation

Tracer molecules

By comparing the differential accumulation of small and large molecule tracers, this experiment was designed to detect the permeability pathways most impacted by IL-6. The small molecule tracers included lucifer yellow (LY; 1 mM) and sodium fluorescein (0.25 mM), which equilibrate quickly outside spheroids [38, 39], as well as AF488-tagged methotrexate (MTX; 2 μM) [39, 40]. AF647-tagged 10-kDa dextran (dextran; 1 mM) served as the large molecule tracer (Fig. 2B-C).

Timelapse confocal microscopy

To quantify tracer accumulation over time, a novel serial confocal microscopy technique (Fig. 2A) was developed based on one previously published [36]. Excitation laser properties were kept constant for each spheroid condition, each tracer, and across all time points. Once experiments began, serial confocal images (every 2–5 min) of each spheroid were collected and subsequently anonymized. Single depth images were used, as the thickness of the Matrigel domes influenced image resolution at varying depths and limited generation of z-stack images. The ratio of interior tracer fluorescence to the exterior value was normalized to the baseline ratio, and this value reflected tracer accumulation over time.

Experimental manipulations for intra-vacuole tracer accumulation

Testing IL-6's sufficiency in clearance deficits, IL-6 WT spheroids were exposed to a single dose of recombinant murine IL-6 (10 ng/mL), egtazic acid (EGTA; 2mM; tight-junction disruption [41], positive control), or PBS of equal volume (negative control). To assess the necessity of IL-6, IL-6 KO MRL/lpr spheroids were compared to those identically derived from the IL-6 WT MRL/lpr strain. Separately, IL-6 signaling was suppressed in IL-6 WT spheroids by a 12-hour pre-incubation with an anti-IL-6-receptor blocking antibody [42] (anti-IL-6-R; 1 μg/mL). Control spheroids were incubated with the manufacturer-recommended IgG2 isotype control antibody (1 μg/mL).

Tracer studies: intra-cellular accumulation due to perturbed ABC transporter function

Tracer molecule

The ABC-specific tracer fluorescein diacetate (FD; 5 μM) is hydrophobic and inert outside of cells, but it moves freely into the cytoplasm where it becomes both fluorescent and hydrophilic. Three types of ABC transporters, P-gp, MRP1, and BCRP, can efflux FD and reduce fluorescence; therefore, a brighter cell cytoplasm reflects decreased ABC clearance.

Spheroid genotypes and ABC transporter inhibitors

First, the baseline FD clearance was compared between unmanipulated IL-6 KO and IL-6 WT spheroids. Next, we assessed the ability of specific ABC inhibitors, including MK571 (55 μM; MRP1 inhibitor) and Novobiocin (100 μM; BCRP inhibitor), to phenocopy any IL-6-mediated effects in IL-6 KO spheroids. Each inhibitor was dissolved in DMSO, so an equal volume of DMSO alone served as the negative control.

Experimental timeline and analysis

Prior to imaging, spheroids were incubated with the ABC inhibitors or DMSO. After a two-hour incubation, FD was added. Ninety minutes later, the spheroids were moved to the confocal microscope for single time point image collection. Images were anonymized, and the single brightest cell body was identified for each spheroid. The average fluorescence of this singular cytoplasmic compartment was measured, and this value was then divided by the average fluorescence within an equally sized region of the nearby extracellular space. This ratio reflected intracellular FD accumulation for the spheroid.

Statistics

All data underwent outlier and normality assessment. Appropriate two-tail parametric (Students T-test) or non-parametric (Mann Whitney U test) means-based comparisons were used ($p < 0.05$ is significant). The sample sizes provided for tracer experiments reflect individual spheroids. We imaged ten spheroids (biological replicates) derived from multiple explanted CPs of the

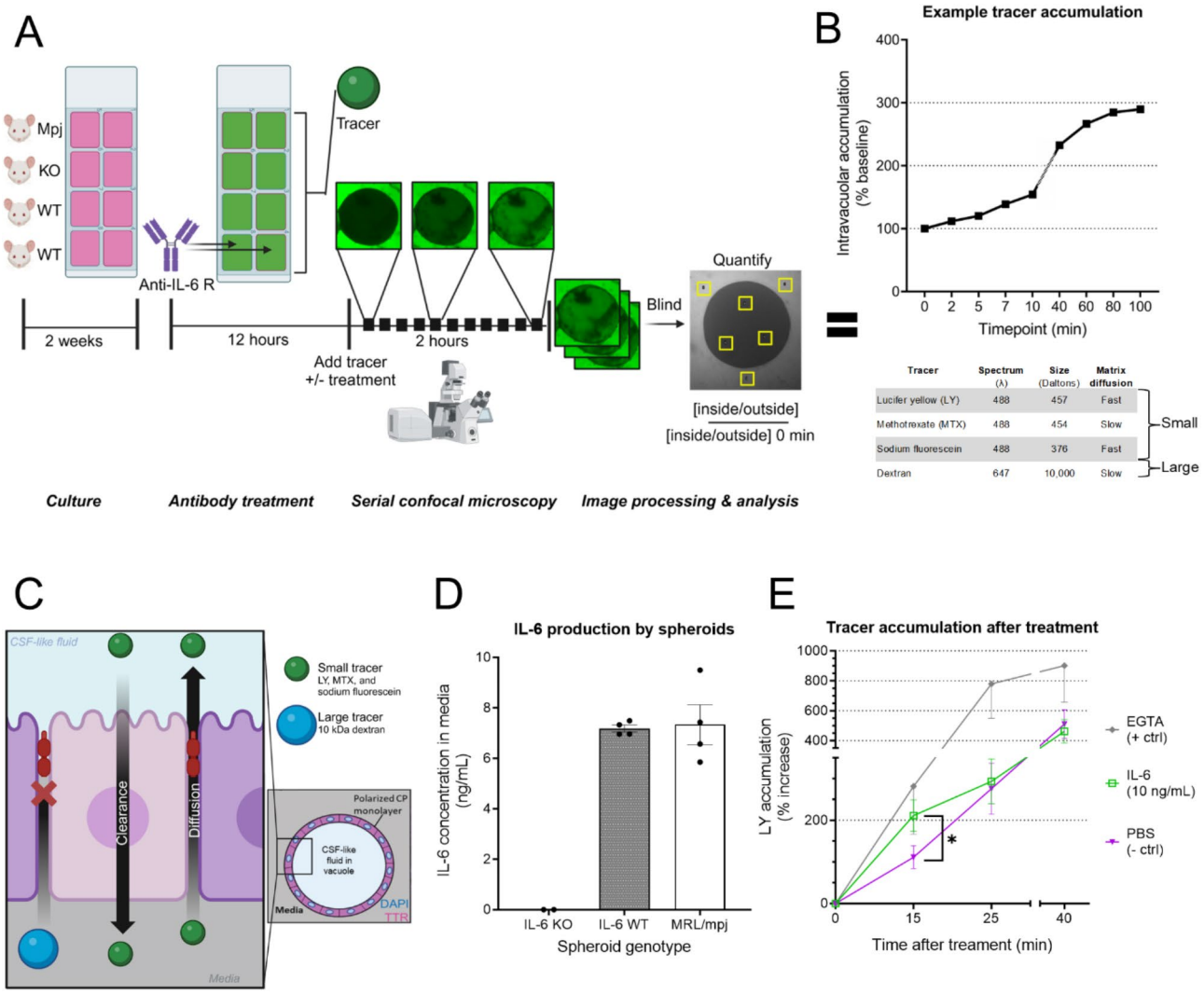

Fig. 2 Exogenous IL-6 suppressed tracer clearance by choroid plexus spheroids. **A)** Experimental design for intra-vacuole accumulation tracer studies. CP spheroids were generated from MRL/Mpj (Mpj), IL-6 knockout (KO) or IL-6 wildtype (WT) MRL/lpr lupus mice. After 2 weeks of culture, IL-6 WT spheroids could be exposed for 12 h to anti-IL-6 receptor (Anti-IL-6-R) or isotype control antibodies to block IL-6 signaling. One of the tracers was added to each well and serial images were acquired every two to five minutes for two hours with a confocal microscope. Following imaging, all images were assigned a randomized number and experimenters were blinded to spheroid genotype and treatment. Fluorescence intensity within three two-dimensional regions of interest (yellow squares) were averaged to quantify inside or outside tracer levels. To quantify tracer accumulation, the inside average was divided by the outside average. That ratio was normalized to a baseline time point. Over time, those tracers that diffused into the vacuole accumulated and produced a time-course like that depicted in the graph (**B**; top graph). Higher intra-vacuole accumulation reflects decreased clearance. Time is plotted in wider intervals at later timepoints to ease visualization of the clearance trend across the full experiment. B, bottom) Table of tracers used in the spheroid experiments, their fluorescence spectrum, molecular size (brackets categorize as small or large), and the expected rates of diffusion through the extracellular matrix. **C)** Schematic depicting the diffusion and clearance of small tracers while highlighting the expectation that large tracers should not permeate spheroids with intact tight junctions. **D)** ELISA-measured levels of IL-6 in the media of wells containing CP spheroids derived from mice of each genotype (IL-6 KO MRL/lpr, IL-6 WT MRL/lpr, or MRL/mpj). As each well contains many spheroids and IL-6 KO spheroids are not expected to express the *il6* gene, IL-6 levels were quantified in the media of only two, rather than four, wells of L-6 KO spheroids. **E)** Accumulation of LY within IL-6 WT spheroids following acute EGTA (positive control), PBS (negative control), or IL-6 (10 ng/mL) exposure. Error bars: standard error mean

same genotype and cultured in a single well (technical replicate). Each pooled explant and its daughter spheroids were used only in one experiment. During blinded image analysis, some spheroids were excluded for poor image quality (i.e., obscured fluorescence by superimposed spheroids or poorly visualized lumen). Spheroid volume and surface area were not found to impact tracer accumulation in validation studies (Supplementary Materials and Methods), so spheroid size was not used as an exclusion criteria in our subsequent experiments. Two or more technical replicates, each with ten spheroids, were used per condition in all LY, sodium fluorescein, and dextran experiments. MTX and FD experiments utilized one technical replicate per condition, as they were designed

to expand upon our preceding LY findings. GraphPad Prism 9 and Microsoft Excel were used to perform all statistical analyses and to produce all graphs.

Results

Characterization of CP spheroids derived from lupus mice

Generally following a protocol used in C57Bl/6J mice [29], we generated functional spheroid models of the CP from primary tissue explants from adult lupus mice (Fig. 1A). As this was the first application described of this (or any other) spheroid technique to the study of the lupus CP, it was necessary to validate our approach. In the interest of experimental expediency, we also assessed if lupus-mouse-derived spheroids could be analyzed earlier than eight weeks, the time point originally published [29].

After two weeks of culture, spheroids displayed the expected morphology and physiology (Fig. 1B-I). These spheroids replicated the in vivo cytoplasmic distribution of transthyretin (TTR; a canonical CP marker; Fig. 1B-D). Within a single 500 µL well on the µ-slides, dozens of spheroids formed (Fig. 1E). While non-epithelial cell types of the CP (i.e., fibroblasts) were possibly present in the explanted tissue, Petersen et al. confirmed that epithelial cells are the dominant cell type [29] and are further selected for by spheroid culture conditions. Our subsequent electron microscopy studies additionally confirmed that epithelial cells are the only constituent of viable, mature spheroids. The epithelial cells displayed clear apical and basolateral polarity which created an internal CSF-like fluid compartment distinct from the external matrix and media. The spheroid epithelium displayed ultrastructural characteristics of the CP epithelia, including intact apical-lateral tight junctions between juxtaposed epithelial cells, apical microvilli, and abundant mitochondria (Fig. 1F-G).

Additionally, two-week old spheroids displayed expression of key genes (including brain creatine kinase, occludin, transferrin, and transthyretin) comparable to that of in vivo CP tissue (Fig. 1H). EGTA exposure, which chelates calcium to disrupt tight junctions, rapidly decreased spheroid size. This collapse is indicative of the loss of paracellular integrity and resulting free flow of fluid between vacuole and media (Fig. 1I).

Next, we utilized tracer studies to understand the impact of IL-6 on spheroid permeability (Fig. 2A-C). As the in vivo CP epithelia can produce IL-6, we queried the capacity of mature spheroids to secrete this cytokine by measuring its levels in the culture media using ELISA (Fig. 2D). As expected, IL-6 KO spheroids did not produce IL-6. The media concentrations of IL-6 were equivalent between spheroids derived from MRL/lpr (IL-6 WT, 7.2 ± 0.1 ng/mL, $n = 4$ wells) or MRL/mpj mice (7.3 ± 0.8 ng/mL, $n = 4$ wells; $p > 0.05$). Taken together, lupus mouse CP spheroids exhibited the expected gene expression, morphology, barrier integrity, and protein secretory capacity.

The impact of IL-6 on tracer accumulation within spheroids

The accumulation of exogenous tracer within their central vacuole could reflect either increased tracer permeation of the spheroids (paracellular diffusion or transcellular secretion) or defective clearance of the tracer from the vacuole [36, 38]. A combination of LY and dextran has previously been used to query paracellular and transcellular permeability of epithelial organoids [43]; MTX was chosen as a lupus drug with similar efflux pathways to LY which would better characterize the potential clinical relevance of CP permeability changes. The ultrastructure of tight junctions exhibit proper alignment (Fig. 1F-G), which supports intact paracellular integrity of the spheroid epithelial barrier. Furthermore, impermeability of spheroids to dextran, described in Sect. 3.3, further supports intact paracellular integrity. Therefore, we assumed that accumulation of exogenous tracer within the central vacuole more likely represents perturbed transcellular clearance function.

Testing the capacity of IL-6 to induce clearance defects, we exposed IL-6 WT spheroids to a single bolus of exogenous IL-6 or control treatments and quantified LY accumulation (Fig. 2E). IL-6 treatment was associated with increases in the average LY accumulation comparable to the positive control EGTA group. IL-6 exposure significantly enhanced LY accumulation at 15 min compared to PBS exposure (IL-6: 211 ± 38% of baseline, $n = 39$; PBS: 111 ± 27% of baseline, $n = 38$; $^{*}p = 0.014$). Later timepoints did not show a similar effect.

To assess changes to LY accumulation in the absence of IL-6, we repeated these tracer studies in IL-6 KO spheroids and compared them to IL-6 WT and MRL/mpj controls. Whereas IL-6 exposure had a rapid and transient effect, IL-6 KO spheroids displayed a long-lasting decrease in LY accumulation relative to IL-6 WT (Fig. 3A-B). Specifically, at five minutes the absence of IL-6 was associated with significantly lower LY accumulation (IL-6 KO: 110 ± 6% of baseline, $n = 31$; IL-6 WT: 126 ± 6% of baseline, $n = 27$; $^{*}p = 0.01$). This effect became even more pronounced at time points beyond 30 min. At 60 min, IL-6 KO spheroids (213 ± 17% of baseline, $n = 31$) displayed lower LY accumulation compared to IL-6 WT (273 ± 14% of baseline, $n = 26$; $^{*}p = 0.01$). Across all timepoints, MRL/mpj spheroids displayed LY accumulation equal to IL-6 WT ($p > 0.05$).

While absence of IL-6 appears to result in higher clearance, we wondered if directly inhibiting IL-6 signaling in IL-6-competent spheroids would have a similar effect. Thus, IL-6 WT spheroids were incubated with IL-6 receptor blocking antibodies (anti-IL-6-R; 1 µg/

mL) or isotype control antibodies for twelve hours prior to the addition of tracer. LY experiments were repeated (Fig. 3C-D), and lower accumulation was observed in the IL-6-receptor-blocked spheroids at 60 min (Anti-IL-6-R: 247 ± 17% of baseline, $n = 17$; Isotype: 418 ± 84% of baseline, $n = 4$; $^{*}p = 0.017$) and later time points. Notably, some of the isotype-treated spheroids were excluded before unblinding due to poor image quality; however, the remaining spheroids displayed minimal variability in average fluorescence, so a smaller sample size was tolerated.

The accumulation-lowering effect of IL-6 receptor blockade was also observed when fluorescently tagged MTX was used rather than LY (Fig. 3E-F). Incidentally, accumulation trends appeared negative in MTX experiments. This tracer was observed to diffuse more slowly through the extracellular matrix than LY, potentially caused by additional interactions between the more anionic MTX molecule and negatively charged proteoglycans in the matrix. In the MTX experiments, sufficient outside fluorescence gathered after 30 min, the baseline time point. Over the subsequent observation period, outside fluorescence continued to increase, which lead to the overall negative slope of the early portion of the graph. At later time points, the slope approaches zero as MTX approaches equal distribution throughout the extracellular matrix and inward diffusion becomes more prominent. Since tracer experiment calibration and analysis compare different spheroid conditions at each time point independently to assess clearance activity, we contend that the negative or positive curve is irrelevant when assessing IL-6's impact.

Lower MTX accumulation was observed in the IL-6 receptor-blocked spheroids compared to isotype controls at 46 min (Anti-IL-6-R: 83 ± 2% of baseline, $n = 10$; Isotype: 92 ± 1% of baseline, $n = 10$; $^{**}p = 0.004$), 60 min (Anti-IL-6-R: 72 ± 4% of baseline, $n = 10$; Isotype: 84 ± 3% of baseline, $n = 10$; $^{**}p = 0.009$), and later time points.

IL-6 and the epithelial paracellular barrier

While LY and MTX clearance was suppressed, no IL-6 related differences were observed in accumulation of sodium fluorescein or dextran (Fig. 3G-H). Due to its large size, dextran equilibrates more slowly through the extracellular matrix than does LY. Therefore, the continued increases in extracellular levels as dextran distributed throughout the observation period (increasing outside accumulation relative to that within the Matrigel) most likely produced the observed negative slope in the accumulation curve, as was seen in the early portion of the MTX curves. However, unlike MTX, the slope of dextran's curves never returned to zero; this particular observation could be attributed to intact paracellular integrity which prevented inward diffusion of the labeled dextran, producing a progressively negative ratio of inside to outside fluorescence. This interpretation is further supported by tight-junction specific studies.

EGTA-exposed spheroids in Fig. 2E exhibited increases in LY accumulation by 15 min (281 ± 115% of baseline, $n = 17$), likely by disrupting tight-junctions. Relative to PBS-treated spheroids (111 ± 27% of baseline, $n = 38$), EGTA-treated spheroids did have a higher average LY accumulation, although this difference did not reach significance. We attribute this near significance to the collapse of many EGTA-treated spheroids prior to the 15-minute time point, both reducing sample size and complicating measurement of vacuole fluorescence. Increases in LY accumulation following EGTA exposure likely resulted from altered entry and exit of LY from the central vacuole, reflecting the disruption of functional tight-junctions.

Supporting the lack of IL-6 effect on paracellular integrity inferred from sodium fluorescein and dextran studies, transmission electron microscopy comparisons of IL-6 KO and IL-6 WT spheroids found no differences in the prevalence, apparent integrity, or achieved cellular apposition of tight-junctions (Fig. 4A-B, left). Additionally, qualitative assessment of other key epithelial cell features (i.e., relative positioning of cells, mitochondria, nuclear integrity and chromatin state, endocytic pit formation, and ciliation) revealed no differences between IL-6 KO and IL-6 WT spheroids (Fig. 4A-B, right).

Furthermore, no differences were observed between MRL/lpr (IL-6 WT) and MRL/mpj spheroids (Fig. 4C). Quantification of microvilli coverage corroborated the lack of qualitive differences observed in the three spheroid genotypes (Fig. 4D; IL-6 WT: 87.7 ± 5.7%; IL-6 KO: 93.1 ± 2.0%; MRL/mpj: 85.8 ± 7.7%; $p > 0.5$). Similarly, quantifying the number of tight junctions per millimeter of circumference showed no difference between genotypes (Fig. 4E; IL-6 WT: 39.2 ± 1.9; IL-6 KO: 54.5 ± 13.1; MRL/mpj: 35.7 ± 13.0; $p > 0.4$).

Taken together, the lupus (MRL/lpr; IL-6 WT) and control (MRL/mpj) spheroids exhibited comparable IL-6 production, tracer accumulation, and macrostructural integrity, which points to their equivalent behavior of the two genotypes in the ex vivo environment. Subsequent IL-6-focused experiments, therefore, used only those spheroids derived from IL-6 WT mice as controls.

Variation in the activity of epithelial ABC transporters related to IL-6

Our observations supporting unaltered paracellular integrity led us to consider that functional changes to transporters could be mediating IL-6's apparent suppression of clearance. Interestingly, the two tracers whose clearance was regulated by IL-6, LY and MTX, are substrates of ABC transporters [44, 45].

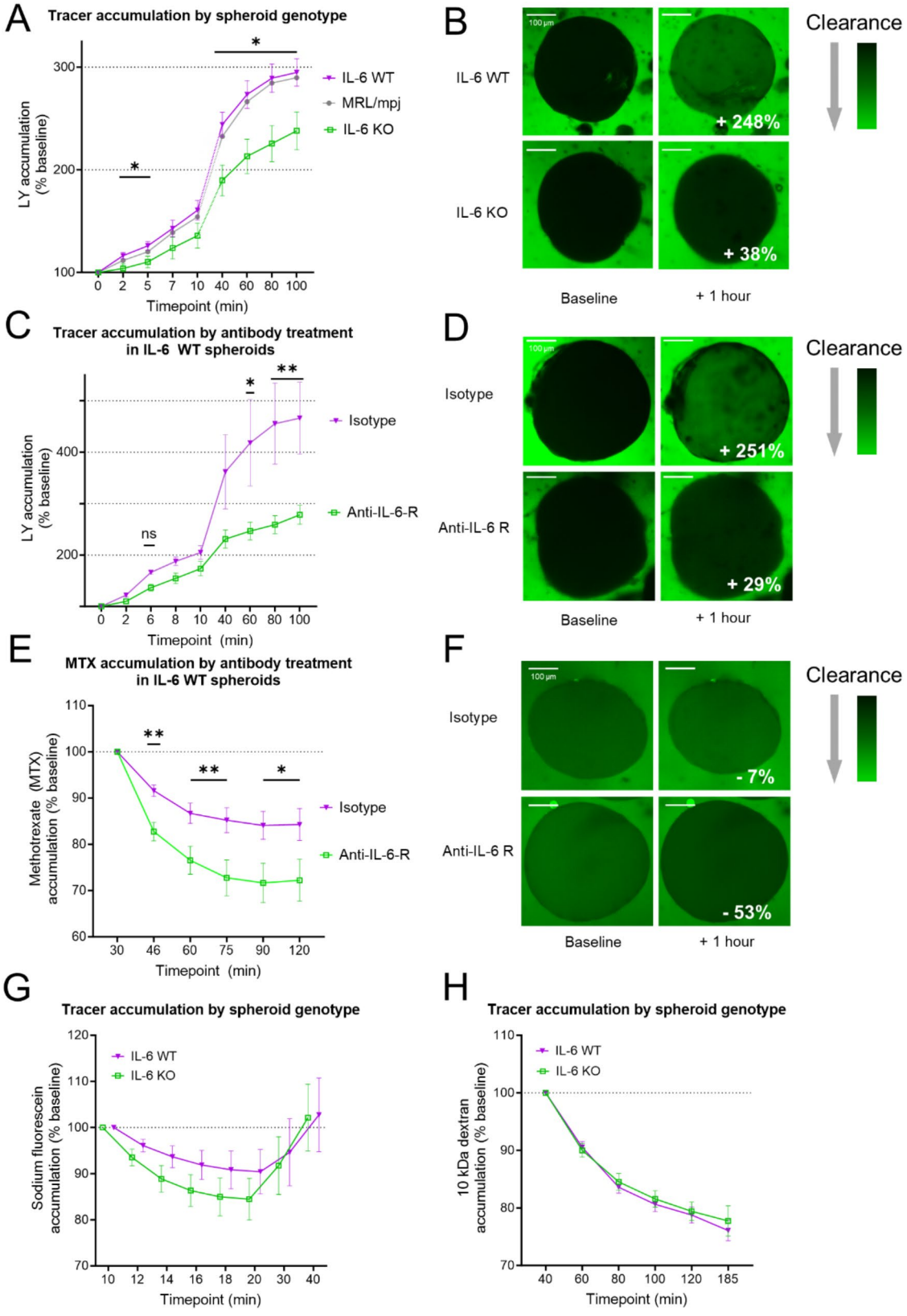

Fig. 3 (See legend on next page.)

(See figure on previous page.)

Fig. 3 Blocking IL-6 signaling increased tracer clearance by choroid plexus spheroids. **(A)** Spheroids generated from IL-6 WT, MRL/mpj, or IL-6 KO MRL/lpr mice received no additional treatment. Lucifer yellow (LY) accumulation in the central vacuole was measured over time to determine baseline differences in clearance. Significance bars indicate comparison between IL-6 WT and IL-6 KO spheroids. **(B)** Representative color change from baseline for spheroids of each genotype after one hour. Change represented as percent increase in intra-vacuole fluorescence. The representative images (top) depict an IL-6 WT spheroid with a 248% increase above baseline in LY accumulation after one hour. The IL-6 KO images (bottom) reflect an spheroid with only a 38% increase above baseline over the same timeframe. **(C)** Spheroids generated from IL-6 WT mice were incubated for twelve hours with anti-IL-6-receptor blocking antibodies (anti-IL-6-R) or isotype control antibodies. LY accumulation over time was quantified. **(D)** Representative color change from baseline of spheroids with antibody treatment. The representative isotype-treated spheroid (top) demonstrated a 251% increase in LY accumulation above baseline over one hour. Compared over the same interval, the spheroid treated with anti-IL-6-R antibodies (bottom) experienced a 29% increase above baseline. **(E)** Methotrexate (MTX) accumulation was assessed in antibody-treated spheroids as in C. **(F)** Representative images of MTX fluorescence change under each condition. A representative isotype-treated spheroid (top) showed a 7% decrease in measured MTX accumulation from baseline over one hour, while the spheroid treated with anti-IL-6-R antibodies (bottom) showed a 53% decrease in MTX accumulation over the same time frame. The negative trend in accumulation under both conditions was due to slower distribution of MTX than LY throughout the matrix, leading to consistently increasing outside fluorescence values. This delayed rise in extracellular fluorescence was thought to occur because of the electrostatic interaction between MTX and the Matrigel. Accumulation of sodium fluorescein **(G)** or dextran **(H)** in spheroids of different genotypes. Increased intra-vacuole fluorescence reflects decreased clearance (arrows and color scale). Scale bars: 100 µm. $^{*}p < 0.05$, $^{**}p < 0.01$. Error bars: standard error mean

In addition to alterations in expression, we studied functional changes to ABC transporters using a modified tracer study paradigm specific to ABC clearance. As described in Methods Sect. 2.8, fluorescent FD is removed from spheroid cell bodies and inactivated only when cleared by ABC transporters (Fig. 5A, left). Therefore, higher fluorescence within the cells lining the spheroid vacuole resulted from deficits in FD clearance (Fig. 5A, right). Under control conditions (Fig. 5B), IL-6 KO spheroids exhibited significantly less FD accumulation (1.6 ± 0.2, $n = 8$) than that of IL-6 WT spheroids (4.3 ± 1.0, $n = 10$, $^{*}p = 0.022$).

To determine both the functional importance of the transporters in the CP and the potential to phenocopy IL-6's apparent suppression of clearance functionality, specific inhibitors were used to block FD clearance by MRP1 and BCRP in IL-6 deficient spheroids (Fig. 5C). IL-6 KO spheroids treated with Novobiocin (BCRP inhibitor) exhibited increased FD accumulation compared to the negative control (DMSO) treated IL-6 KO spheroids (Novobiocin: 4.8 ± 1.2, $n = 10$; DMSO: 1.6 ± 0.2, $n = 8$; $^{*}p = 0.031$). Similarly, MK571 (MRP1 inhibitor) treatment increased FD accumulation within IL-6 KO spheroids relative to controls (MK571: 3.7 ± 0.7, $n = 9$; DMSO: 1.6 ± 0.2, $n = 8$; $^{*}p = 0.016$). Therefore, either BCRP or MRP1 inhibition increased IL-6 KO spheroid FD accumulation to a comparable level with that of IL-6 exposure.

The influence of IL-6 on ABC transporter expression in lupus mice

To determine the translational impact of these ex vivo findings, in vivo expression of genes encoding constituent proteins of the three primary ABC transporters (P-gp, MRP1, and BCRP) was measured in the CP of IL-6 KO and IL-6 WT lupus mice (Fig. 6A). P-gp expression did not differ between the genotypes (IL-6 KO: 1.5 ± 0.2, $n = 7$; IL-6 WT: 1.6 ± 0.3, $n = 7$; $p = 0.999$). MRP1 expression was higher on average in IL-6 KO mice but not significantly so (IL-6 KO: 8.3 ± 1.4, $n = 7$; IL-6 WT: 6.4 ± 0.9, $n = 7$; $p = 0.259$). BCRP expression, however, was significantly elevated in IL-6 KO mice (2.8 ± 0.3, $n = 6$) compared to IL-6 WT mice (1.8 ± 0.2, $n = 6$; $^{*}p = 0.026$).

Similarly, evaluation of BCRP using immunofluorescent staining found increased levels of this transporter in the CP of IL-6 KO mice compared to IL-6 WT mice (Fig. 6B-C; IL-6 KO: 3.5 ± 0.4, $n = 8$; IL-6 WT: 2.4 ± 0.3, $n = 8$; $^{*}p = 0.028$).

Discussion

Using ex vivo CP spheroids, we observed the capacity of IL-6 to suppress epithelial cell clearance of the ABC transporter substrates LY and MTX and demonstrated the direct role of IL-6 signaling in these clearance reductions. CP epithelial BCRP and MRP1 were identified as the primary ABC transporters impacted by IL-6, while BCRP expression in vivo supported the translational relevance in lupus mice. Taken together, these findings indicate IL-6's potential disruption of blood-CSF barrier clearance functions in conditions (such as NPSLE) with high systemic and CNS levels of this inflammatory cytokine.

IL-6 suppresses BCRP and MRP1 function at the CP

IL-6 could act in both autocrine and paracrine fashions to influence CP physiology. Exogenous IL-6 exposure acutely suppressed LY clearance, and, correspondingly, IL-6 KO spheroids exhibited enhancement of LY clearance, while blocking the IL-6R receptor phenocopied this effect. Therefore, IL-6 signaling through IL-6R likely suppressed clearance of LY. Studies with MTX demonstrated similar restoration of clearance by blocking the IL-6R, suggesting that the clearance mechanism affected by IL-6 must preferentially transport LY and MTX.

ABC transporters are vital to clearance activity by the CP epithelium [13]. Among their key substrates, BCRP avidly transports LY, while MRP1 transports LY to a lesser extent [46]. MTX and FD are substrates of both BCRP and MRP1 [15]. However, neither transporter

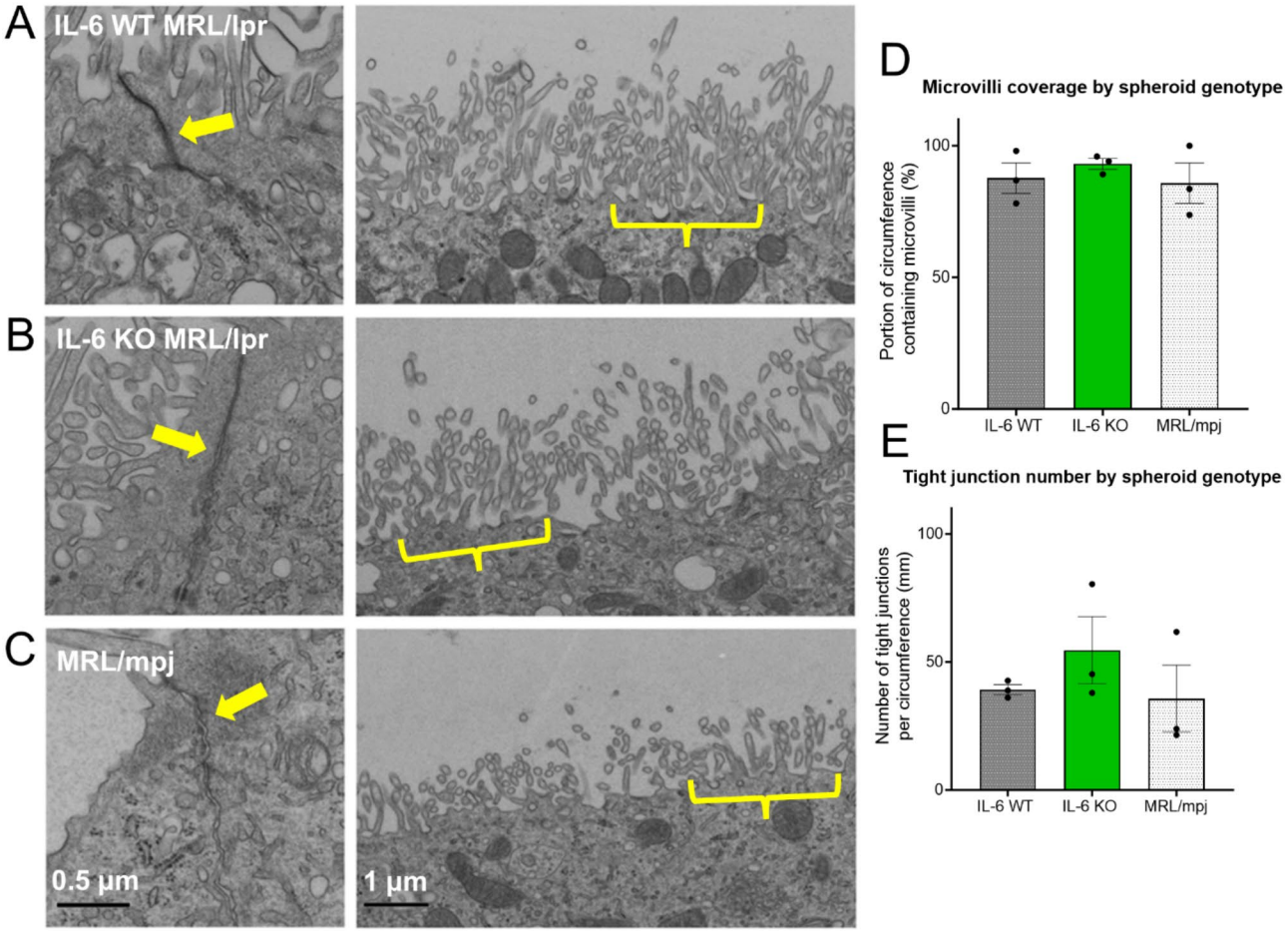

Fig. 4 Structural components of choroid plexus spheroids were unaffected by IL-6. Transmission electron microscopy images of spheroids were compared between each explant genotype ($n = 3$ for each strain). Key epithelial components were compared between spheroids from IL-6 WT MRL/lpr **(A)**, IL-6 KO MRL/lpr **(B)**, or MRL/mpj mice **(C)**. Representative images highlight inter-epithelial tight junctions (left; arrows) and apical microvilli (right; brackets). To correct for variation in the size of imaged spheroids, each spheroid's circumference was measured. Next, the percentage of total circumference covered in microvilli **(D)** and the number of tight junctions per unit circumference **(E)** were calculated for each spheroid and compared between genotypes

significantly transports sodium fluorescein [44–46], which can explain the surprising absence of sodium fluorescein accumulation changes associated with IL-6. P-gp plays a minor role in the CP [47], which combined with our findings of minimal P-gp expression in vivo justified our prioritization of BCRP and MRP1 in our functional studies.

We next employed an ABC-specific tracer, FD, and specific inhibitors to dissect the functional interaction between IL-6, BCRP, MRP1, and CP spheroid clearance activity. At baseline, IL-6 deficient spheroids cleared more FD, indicating once again that IL-6 decreases normal clearance by ABC transporters. When IL-6 KO spheroids were treated with inhibitors of either BCRP or MRP1, they exhibited comparable clearance defects to IL-6 WT spheroids. Subsequent in vivo evaluation found that IL-6 deficiency corresponded to significantly higher expression of BCRP, while MRP1 expression trended higher as well. Follow up immunofluorescent staining corroborated this BCRP increase in IL-6 deficient mice. IL-6 has previously been shown to suppress ABC transporter expression in hepatocytes [48], and here we show a similar effect in the CP epithelial cells.

Potential limitations to this interpretation could include the possibility that tracer accumulation may result from either decreased clearance or increased entry of tracer. The dominant intake mechanism of LY in CP epithelial cells remains unclear. Moreover, the primary influx pathway of MTX in vascular endothelial cells, the reduced folate carrier (RFC), appears to be less expressed in native CP epithelial cells [49]. However, we clearly observed the accumulation of both tracers in the central lumen of control spheroids. Passive paracellular diffusion regulated by tight junctions appeared undisturbed as well, as evidenced by the relative impermeability to dextran and intact ultrastructure. Future studies could employ smaller

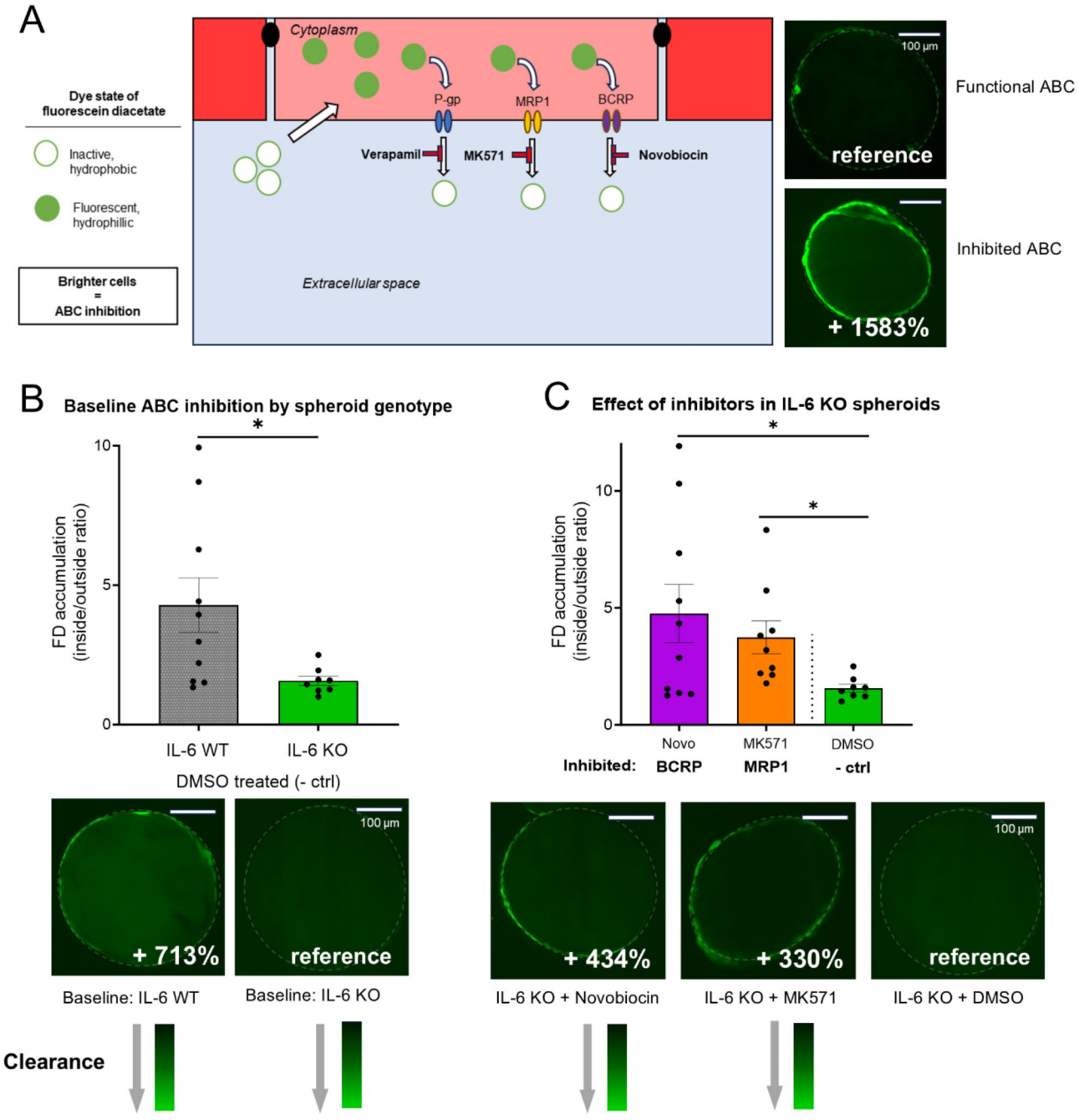

Fig. 5 IL-6 suppressed clearance activity of the ABC transporters BCRP and MRP1. The EFFLUX-ID green multi-drug resistance kit was used to specifically assess ABC transporter functions in spheroids. (A) Schematic of ABC experiment (left). Fluorescein diacetate (FD) in its fluorescently inactive state freely moves across cell membranes. Once inside the cell, cytoplasmic enzymes convert it to its active and hydrophilic state. ABC transporters are the only efflux and inactivation mechanism of FD. Several inhibitors (e.g., MK571, Novobiocin) can be used to block individual ABC efflux of FD to determine the important transporters in spheroid clearance. As a result, those spheroids with suppressed ABC transporter function display more intense fluorescence due to trapping of active FD within the epithelial cells lining the spheroid vacuole (**A**, bottom right panel). **(B)** Rather than timelapse imaging, single images were collected at 90 min following FD addition to media as no time-dependent changes were anticipated. Accumulation was measured as fluorescence intensity of the brightest cell body within each spheroid, relative to fluorescence intensity of the extracellular space (inside/outside ratio). **B**, top) FD accumulation in IL-6 WT and IL-6 KO spheroids without inhibitor treatment (DMSO, negative control). **B**, bottom) Representative images provide a view of an IL-6 KO spheroid with intact ABC clearance (right) compared to an IL-6 WT spheroid with 713% more FD accumulation (left). **(C)** IL-6 KO spheroids were exposed to Novobiocin or MK571 to determine if inhibiting either of the two CP-relevant ABC transporters, BCRP or MRP1, could induce clearance defects like those in IL-6 WT spheroids. **C**, top) Average FD accumulation under each inhibitor was compared. **C**, bottom) Compared to the reference image (right panel), the provided image of a Novobiocin-treated IL-6 KO spheroid exhibits 434% more FD accumulation (left panel). A representative image of an MK571-treated IL-6 KO spheroid (middle panel) shows 330% more FD accumulation compared to the reference image. Increased cellular fluorescence represented decreased clearance (arrows and color scale). Scale bars: 100 µm. $^{*}p < 0.05$. Error bars: standard error mean

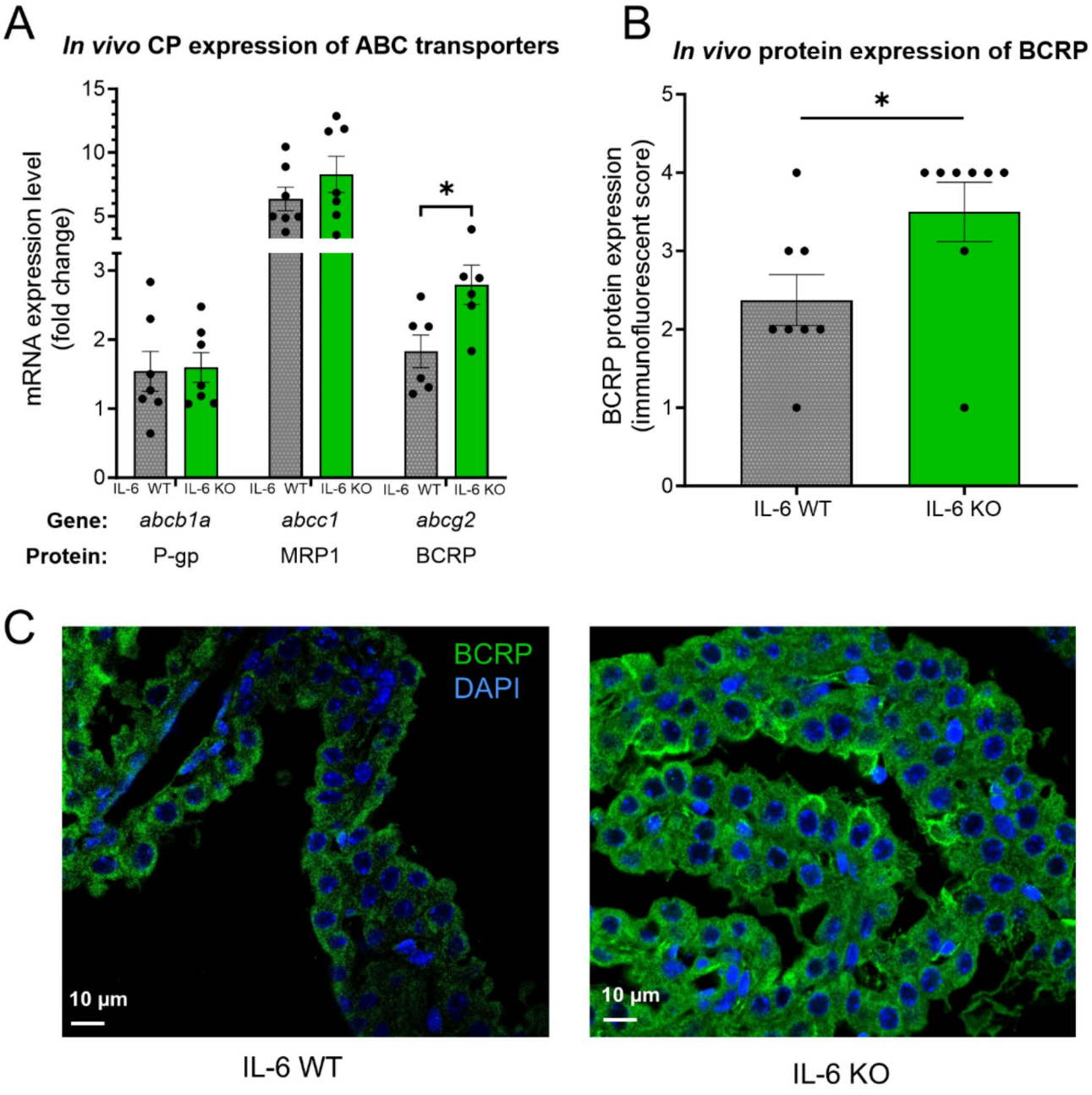

Fig. 6 IL-6 expression altered transporter expression in the lupus mouse choroid plexus. **(A)** Real time quantitative PCR was used to measure in vivo expression of ABC transporter genes in the CP of IL-6 WT or IL-6 KO MRL/lpr mice. Gene names and corresponding ABC transporter subtype are provided. **(B)** Comparison of immunofluorescent labeling of BCRP in CP sections collected from IL-6 WT and IL-6 KO MRL/lpr mice. **(C)** Representative images of BCRP immunofluorescence (60x magnification). *$p < 0.05$. Error bars: standard error mean

dextrans (3–5 kDa) to assess unanticipated size thresholds for junctional integrity. Nonetheless, combined influx through multiple minor transcellular pathways, including low-level RFC activity, organic anion transporter influx, and trans-membrane diffusion [50–52], may explain LY and MTX accumulation, which is then resisted by clearance through pathways permissive to sodium fluorescein but selective for LY and MTX. ABC transporter clearance changes regulated by IL-6, then, likely best explain these findings.

While we cannot exclude the contribution of transporter-mediated influx to LY and MTX accumulation, the FD finding of baseline ABC clearance inhibition by IL-6 strengthens our conclusion that disrupted clearance leads to accumulation of LY and MTX in IL-6 exposed spheroids. Furthermore, either BCRP or MRP1 inhibition can replicate the IL-6 effect on clearance. In future

studies, measuring FD accumulation in IL-6 KO spheroids cultured in the presence of IL-6 could prove additional confirmation. This can be done through addition of the cytokine to the culture media, but the effect of IL-6 may vary with time and in such an experimental setup only a single time point is captured. Alternatively, a technique which delivers continuous IL-6 (e.g. by viral transfection) would be needed to mirror the conditions of the IL-6 WT spheroids which continuously secrete the cytokine. Despite this limitation, we believe the balance of our findings convincingly support the negative impact of IL-6 on clearance function. Additional follow up studies can also further tease apart IL-6's specific impacts on BCRP and MRP1 over short and long-term timeframes of exposure. Nonetheless, we have detected a novel B-CSFB-altering interaction between IL-6, a cytokine implicated in NPSLE, and the CP's removal of ABC substrates from the CSF.

Interactions between IL-6, ABC transporters, and the CP

While a specific intracellular mechanism linking IL-6R signaling to modulation of either MRP1 or BCRP is still under investigation, our results indicate both a prompt and long-term impact on these ABC transporters. As to how the early effect occurs, protein kinase activity quickly regulates ABC function [53–55]. Interestingly, inflammatory conditions which promote inducible nitric oxide synthase and subsequent protein kinase C activation, including TNF or LPS, demonstrate a rapid (< 30 min) detrimental effect on ABC transporter efflux functions in endothelial cells [55]. Since IL-6 activates nitric oxide synthase [56], a similar kinase-mediated effect could explain the quick decrease in clearance observed in IL-6 exposed spheroids.

In contrast, the long-term impacts of IL-6 could relate to reductions in ABC transporter expression [55], an effect we likely observed in the increased expression of BCRP expression in IL-6 KO mice, which could be mediated by MAPK/ERK or PI3K/Akt pathway signaling [48, 55, 57, 58]. Alternatively, IL-6 could suppress membrane trafficking of ABC transporters, which would reduce the CP's functional capacity to clear BCRP and MRP1 substrates. A dose-dependent effect of IL-6 on ABC transporters in vivo could be characterized using MRL/lpr and MRL/mpj mice, which can both produce systemic IL-6 but do so at different levels [59]. Moreover, a key future direction is to discern how exactly IL-6 suppresses CP clearance in the hopes of identifying targeted strategies to restore CP function.

Our findings also contribute to the understanding of normal ABC function in the CP. We confirmed low P-gp expression in the CP, with MRP1 being the most highly expressed [47]. Regarding the polarity of these transporters in the CP, MRP1 is largely regarded to localize to the basolateral membrane and to efflux luminal molecules to the serum [47], while the expression and localization of BCRP in the CP is less clear [13]. Some studies point to an apical localization for the transporter [47], which complicates interpretation of the directionality of BCRP's transport. Our in vivo staining pointed to both apical and basolateral localization of BCRP, although our attempts to localize precisely BCRP in the spheroid model were unsuccessful due to the poor optical properties of Matrigel. We unsuccessfully attempted to utilize Cell Recovery Solution (Corning), thermal dissolution through cooling, and physical agitation to thin the Matrigel and improve spheroid visualization. Despite this limitation, our in vivo staining and tracer experiments aid in clarifying the nature of BCRP. Among the ABC transporters, BCRP is the primary transporter for LY [46], and our functional results point to IL-6 mediated disruption of LY efflux through BCRP. This conclusion favors an apical to basolateral direction of transport mediated by BCRP, although this will need to be confirmed.

Comparison of lupus vs. control derived CP spheroids

In NPSLE patients as well as in animal models of the disease, the CP displays marked inflammatory changes, including infiltration by immune cells [16, 17, 34]. To assess long-lasting impacts of this prominent lupus pathology, we cultured CP spheroids from MRL/lpr and MRL/mpj mice, predicting that structural and functional changes would be evident. However, comparable IL-6 production, TEM-imaged ultrastructure, and LY tracer accumulation indicated that disease-associated differences were not present between the strains in culture. As such, our subsequent experiments prioritized the assessment of the impact of IL-6 and the behavior of specific tracers, including MTX, dextran, and FD, and they did not include an MRL/mpj control group.

We believe that culturing spheroids for two weeks removed the CP tissue from the in vivo lupus-like environment and likely obscured MRL/lpr versus MRL/mpj differences. To overcome this limitation, spheroids could be cultured in the presence of lupus mouse serum or CSF, although perturbed concentrations of vital pro-epithelial cytokines could unpredictably alter the composition of spheroids or survival of residual tissue within the wells. Regardless, MRL/lpr-derived spheroids secreted IL-6 into their own media. As a result, they were consistently exposed to IL-6. The IL-6 KO MRL/lpr mouse was therefore utilized to test spheroid changes in the absence of IL-6, one of the most prominent putative mediators and potential biomarkers of NPSLE.

Etiologic and therapeutic potential in NPSLE

One important potential clinical implication of our results is that potentially toxic accumulation of

anti-rheumatic drugs could be occurring in the CNS of lupus patients with high serum IL-6. We observed IL-6's association with the accumulation of MTX within the CSF-space of spheroids. Another frequently used lupus medication, cyclophosphamide, is similarly cleared by ABC transporters [60]. While we are unaware of studies that have quantified CSF levels of either drug in lupus patients, both MTX and cyclophosphamide have known neurotoxic effects [61–64]. Therefore, accumulation of medications in the CNS could in fact be compounding ongoing neuronal pathology. Currently, CNS bioavailability of lupus medications is not clinically considered in NPSLE. Significant work would still be required first to validate that MTX or cyclophosphamide is accumulating and that these accumulations correspond to exacerbated NPSLE features.

Potentially germane to the pathogenesis of NPSLE, our findings also indicate that IL-6 could be suppressing CP clearance of endogenous neurotoxic metabolites. For example, leukotrienes, which are lipids cleared by MRP1 [65], have previously been shown to activate glial cells [66–68] and to relate to murine cognitive dysfunction in the setting of persistent neuroinflammation [69]. Additional organic compounds cleared by BCRP [15], porphyrins have been shown to decrease neuron growth and survival in vitro and are associated with encephalopathy [70, 71]. In NPSLE, there are signs of gliosis and neuron death [72–75]. The accumulation of endogenous neurotoxins in the CNS, because of decreased ABC clearance at the CP, could be promoting these pathologic changes in NPSLE.

Applicability of CP spheroids to study B-CSFB changes in lupus and other diseases

While recent insights indicate that CP physiology varies based on the ventricular location [76], both our protocol and that previously published by the Petersen group [29] pooled the lateral and 4th ventricular CP to achieve sufficient tissue mass for explant. Ventricle-specific differences likely did not influence our group comparisons, as the thorough mixing of each explant sample should ensure an equal number of lateral and 4th ventricle-derived spheroids in each well regardless of spheroid genotype or exposure. Similarly, by pooling the explants from multiple mice of the same genotype, we may have limited our ability to assess the biological variability within each genotype. This concession was however warranted to yield sufficient tissue mass for successful spheroid generation. Moreover, the reproducible effect of IL-6 across our experimental manipulations, which each used several unique explants per genotype, assured that our findings accurately reflect the biological effects of this cytokine across individuals.

Petersen and colleagues cultured spheroids for eight weeks to carry out immune cell migration studies, while we found that two weeks of culture established in vivo-comparable spheroid morphology and gene expression which were sufficient for assessing barrier integrity to molecules rather than cells. Additionally, the larger size of spheroids in our study is likely due to the larger size, CP mass, and CSF volume of MRL mice compared to the C56BL/6J mice used originally. Another difference between the original and modified protocols is that the two-week procedure did not require passage of spheroids to new plates. Explanted CP tissue contains various cell types in addition to the epithelial cells of interest [76]. Though residual stromal cells from the explant could be present within wells, several technical steps were taken to minimize their influence on epithelial functions: (1) during CP collection, visible fibrous tissue and vasculature were separated; (2) spheroid media contained epithelia-selective cytokines and cytosine arabinoside; and (3) prior to plating, Matrigel-explant suspensions were mixed to ensure homogenous composition across wells. Finally, we strove to control other experimental variations by combining data from spheroids of the same group plated in different wells.

The spheroid model initially described by Petersen et al. and now further expanded to MRL/lpr mice has wide ranging applications. Future lupus investigations can query any number of relevant cytokines for their impact on CP function. Alternatively, the protein synthetic and secretory capacity of the CP can be studied. Beyond lupus, developmental roles of the CP and its neurotrophic factors, a quickly advancing field [77], might be studied using this culture model in fetal mice. By validating that two-week-old spheroids are viable for tracer-based paradigms, we substantiated this model as a reliable and efficient method to study specific CP permeability to molecules and drugs. Applications extend far beyond lupus research, and future experiments could inform drug design or therapy selection to limit or optimize CNS bioavailability.

Conclusions

Given findings from clinical studies and basic research, disruption of blood-CSF barrier integrity likely occurs secondary to CP inflammation in NPSLE. To overcome difficulties limiting the in vivo study of the CP, we studied ex vivo CP spheroids generated from lupus mice. Furthermore, we aimed to discern IL-6's particular role in potential changes to CP function. We successfully generated spheroids from CP tissue explanted from MRL/lpr lupus mice with or without *il6* gene deletion and control MRL/mpj mice. Using a series of tracer studies, we uncovered IL-6's suppression of clearance activities performed by the ABC transporters BCRP and MRP1.

Under the high IL-6 levels in NPSLE, this suppression could hinder the CP's ability to remove neurotoxic molecules from the CSF. Additionally, we directly observed the capacity of IL-6 to suppress CP clearance of methotrexate, a lupus drug with neurotoxic effects. Accumulation of these metabolites or drugs in the brain could propagate neurologic pathology in NPSLE or at least partly counteract the expected therapeutic benefits. These findings represent a new and promising avenue of investigation for basic and clinical studies seeking to elucidate the pathogenesis of NPSLE. Beyond lupus, the spheroid model explored by our studies could be translated to investigations of any number of diseases with apparent CP pathology, with applications that extend to CNS development and drug design as well.

Abbreviations

ABC	ATP-binding cassette transporter
anti-IL-6-R	anti-IL-6-receptor blocking antibody
BCRP	Breast cancer resistance protein
B-CSFB	Blood-CSF barrier
CP	Choroid plexus
CSF	Cerebrospinal fluid
DMSO	Dimethyl sulfoxide
EGTA	Egtazic acid
FD	Fluorescein diacetate
IL-6	Interleukin-6
IL-6 KO	IL-6 knockout
IL-6 WT	IL-6 wildtype
LY	Lucifer yellow
MRP1	Multi-drug resistance protein 1
MTX	Methotrexate
NPSLE	Neuropsychiatric SLE
P-gp	P-glycoprotein
qPCR	Quantitative polymerase chain reaction
SLE	Systemic lupus erythematosus
TTR	Transthyretin

Supplementary Information

The online version contains supplementary material available at https://doi.org/10.1186/s12987-025-00628-x.

Supplementary Material 1

Acknowledgements

We would like to acknowledge Dr. Natalia Petersen (Novo Nordisk) for her collaboration efforts and valuable guidance in establishing the spheroid technique. Additionally, we are grateful to the Analytical Imaging Facility at AECOM and particularly Frank Macaluso for his contributions to evaluating and interpreting the electron microscopy data. We would also like to thank Dr. Anne Muesch and Dr. David Spray at AECOM for their helpful insight into the tracer experiments. Portions of this data were presented the 2022 and 2023 annual meetings of the American College of Rheumatology and Society of Neuroscience by JAR and CP.

Author contributions

Conceptualization, J.A.R., A.B.Z., C.P.; model generation, J.A.R., L.T., C.P.; data curation, J.A.R., L.C., A.D.S.; formal analysis, J.A.R., A.B.Z., C.P.; writing—original draft preparation, J.A.R., C.P.; writing—review and editing, J.A.R., L.T., L.C., A.D.S., A.B.Z., C.P.; visualization, J.A.R.; supervision, A.B.Z., C.P.

Funding

This research did not receive any specific grant from funding agencies in the public, commercial, or not-for-profit sectors. Institutional sources were not involved in the design, conduct, analysis, or reporting of this study. Trainee support to JAR provided by the Medical Scientist Training Program: T32-GM149364. Equipment and services at the AECOM Analytical Imaging Facility used in this study are partially supported by NCI grant P30CA013330 and Shared Instrumentation grants 1S10OD18218-1 and 1S10OD016214-01A1.

Data availability

Data is provided within the manuscript or supplementary information files.

Declarations

Ethics approval and consent to participate

Ethical approval regarding human participants was not required, as no patient samples or data were used in conducting this study. All animal welfare policies and procedures were approved by the Institutional Animal Care and Use Committees at the Albert Einstein College of Medicine (New York). Study reporting and conduct followed the ARRIVE guidelines.

Competing interests

No authors have competing interests, financial or otherwise. At the time of conducting the study, L.T. was an employee of Novo Nordisk A/S.

Production of graphics and image licenses

Graphics used in Fig. 1A A-C were generated using Biorender online software. Reproduction licenses were granted and are available upon request.

Author details

[1]Department of Neuroscience, Albert Einstein College of Medicine, New York, NY, USA
[2]In vitro Obesity research, Global Obesity Research, Novo Nordisk A/S, Måløv, Denmark
[3]Section for Experimental Animal Models, Department of Veterinary and Animal Sciences, University of Copenhagen, Frederiksberg, Denmark
[4]Analytical Imaging Facility, Albert Einstein College of Medicine, New York, NY, USA
[5]Department of Neurological Surgery, Montefiore Medical Center-Albert Einstein College of Medicine, New York, NY, USA
[6]Department of Developmental Biology and Cancer Research, Faculty of Medicine, Hubert H. Humphrey Center for Experimental Medicine and Cancer Research, The Institute for Medical Research Israel-Canada, Hebrew University of Jerusalem, Jerusalem, Israel
[7]Departments of Medicine and Microbiology & Immunology, Albert Einstein College of Medicine, New York, NY, USA
[8]Azrieli Faculty of Medicine of Bar-Ilan University, Zefat, Israel

Received: 10 June 2024 / Accepted: 29 January 2025
Published online: 11 February 2025

References

1. Nusbaum JS, Mirza I, Shum J, Freilich RW, Cohen RE, Pillinger MH et al. Sex Differences in Systemic Lupus Erythematosus: Epidemiology, Clinical Considerations, and Disease Pathogenesis. Mayo Clin Proc. 2020;95(2):384– 94.
2. Somers EC, Marder W, Cagnoli P, Lewis EE, DeGuire P, Gordon C, et al. Population-based incidence and prevalence of systemic lupus erythematosus: the Michigan Lupus Epidemiology and Surveillance program. Arthritis Rheumatol. 2014;66(2):369–78.
3. Jeltsch-David H, Muller S. Neuropsychiatric systemic lupus erythematosus: pathogenesis and biomarkers. Nat Rev Neurol. 2014;10(10):579–96.
4. Kivity S, Agmon-Levin N, Zandman-Goddard G, Chapman J, Shoenfeld Y. Neuropsychiatric lupus: a mosaic of clinical presentations. BMC Med. 2015;13(1):43.
5. Hanly JG, Kozora E, Beyea SD, Birnbaum J. Nervous system disease in systemic Lupus Erythematosus: current status and future directions. Arthritis Rheumatol. 2019;71(1):33–42.
6. Schwartz N, Stock AD, Putterman C. Neuropsychiatric lupus: new mechanistic insights and future treatment directions. Nat Rev Rheumatol. 2019;15(3):137–52.

7. Monahan RC, Inglese F, Middelkoop H, van Buchem M, Huizinga TW, Kloppenburg M et al. White matter hyperintensities associate with cognitive slowing in patients with systemic lupus erythematosus and neuropsychiatric symptoms. RMD Open. 2021;7(2).
8. Sibbitt WL Jr., Brooks WM, Kornfeld M, Hart BL, Bankhurst AD, Roldan CA. Magnetic resonance imaging and brain histopathology in neuropsychiatric systemic lupus erythematosus. Semin Arthritis Rheum. 2010;40(1):32–52.
9. Lindblom J, Mohan C, Parodis I. Biomarkers in neuropsychiatric systemic lupus erythematosus: a systematic literature review of the last decade. Brain Sci. 2022;12(2).
10. Duarte-Delgado NP, Vásquez G, Ortiz-Reyes BL. Blood-brain barrier disruption and neuroinflammation as pathophysiological mechanisms of the diffuse manifestations of neuropsychiatric systemic lupus erythematosus. Autoimmun rev. 2019;18(4):426–32.
11. Spector R, Keep RF, Robert Snodgrass S, Smith QR, Johanson CE. A balanced view of choroid plexus structure and function: focus on adult humans. Exp Neurol. 2015;267:78–86.
12. Damkier HH, Brown PD, Praetorius J. Cerebrospinal fluid secretion by the Choroid Plexus. Physiol Rev. 2013;93(4):1847–92.
13. Ghersi-Egea JF, Strazielle N, Catala M, Silva-Vargas V, Doetsch F, Engelhardt B. Molecular anatomy and functions of the choroidal blood-cerebrospinal fluid barrier in health and disease. Acta Neuropathol. 2018;135(3):337–61.
14. Sturgeon C, Fasano A. Zonulin, a regulator of epithelial and endothelial barrier functions, and its involvement in chronic inflammatory diseases. Tissue Barriers. 2016;4(4):e1251384–e.
15. Gameiro M, Silva R, Rocha-Pereira C, Carmo H, Carvalho F, Bastos ML et al. Cellular models and in Vitro assays for the screening of modulators of P-gp, MRP1 and BCRP. Molecules. 2017;22(4).
16. Gelb S, Stock AD, Anzi S, Putterman C, Ben-Zvi A. Mechanisms of neuropsychiatric lupus: the relative roles of the blood-cerebrospinal fluid barrier versus blood-brain barrier. J Autoimmun. 2018;91:34–44.
17. Stock AD, Der E, Gelb S, Huang M, Weidenheim K, Ben-Zvi A et al. Tertiary lymphoid structures in the choroid plexus in neuropsychiatric lupus. JCI Insight. 2019;4(11).
18. Gueye M, Preziosa P, Ramirez GA, Bozzolo EP, Canti V, Margoni M et al. Choroid plexus and perivascular space enlargement in neuropsychiatric systemic lupus erythematosus. Mol Psychiatry. 2023.
19. Bravi B, Melloni EMT, Paolini M, Palladini M, Calesella F, Servidio L, et al. Choroid plexus volume is increased in mood disorders and associates with circulating inflammatory cytokines. Brain Behav Immun. 2023;116:52–61.
20. Fragoso-Loyo H, Richaud-Patin Y, Orozco-Narváez A, Dávila-Maldonado L, Atisha-Fregoso Y, Llorente L, et al. Interleukin-6 and chemokines in the neuropsychiatric manifestations of systemic lupus erythematosus. Arthritis Rheum. 2007;56(4):1242–50.
21. Trysberg E, Carlsten H, Tarkowski A. Intrathecal cytokines in systemic lupus erythematosus with central nervous system involvement. Lupus. 2000;9(7):498–503.
22. Shimada A, Hasegawa-Ishii S. Increased cytokine expression in the choroid plexus stroma and epithelium in response to endotoxin-induced systemic inflammation in mice. Toxicol Rep. 2021;8:520–8.
23. Bruewer M, Luegering A, Kucharzik T, Parkos CA, Madara JL, Hopkins AM, et al. Proinflammatory cytokines disrupt epithelial barrier function by apoptosis-independent mechanisms. J Immunol. 2003;171(11):6164–72.
24. Walsh SV, Hopkins AM, Nusrat A. Modulation of tight junction structure and function by cytokines. Adv Drug Deliv Rev. 2000;41(3):303–13.
25. Jeltsch-David H, Muller S. Neuropsychiatric systemic lupus erythematosus and cognitive dysfunction: the MRL-lpr mouse strain as a model. Autoimmun Rev. 2014;13(9):963–73.
26. Gulinello M, Putterman C. The MRL/lpr mouse strain as a model for neuropsychiatric systemic lupus erythematosus. J Biomed Biotechnol. 2011;2011:207504.
27. Shipley FB, Dani N, Xu H, Deister C, Cui J, Head JP, et al. Tracking Calcium Dynamics and Immune Surveillance at the Choroid Plexus Blood-Cerebrospinal Fluid Interface. Neuron. 2020;108(4):623–e3910.
28. Erb U, Schwerk C, Schroten H, Karremann M. Review of functional in vitro models of the blood-cerebrospinal fluid barrier in leukaemia research. J Neurosci Methods. 2020;329:108478.
29. Petersen N, Torz L, Jensen KHR, Hjortø GM, Spiess K, Rosenkilde MM. Three-dimensional explant platform for studies on Choroid Plexus Epithelium. Front Cell Neurosci. 2020;14(108).
30. Cash H, Relle M, Menke J, Brochhausen C, Jones SA, Topley N, et al. Interleukin 6 (IL-6) deficiency delays lupus nephritis in MRL-Faslpr mice: the IL-6 pathway as a new therapeutic target in treatment of autoimmune kidney disease in systemic lupus erythematosus. J Rheumatol. 2010;37(1):60–70.
31. Brick JE, Ong SH, Bathon JM, Walker SE, O'Sullivan FX, DiBartolomeo AG. Anti-histone antibodies in the serum of autoimmune MRL and NZB/NZW1 F1 mice. Clin Immunol Immunopathol. 1990;54(3):372–81.
32. Reynolds JA, Li Y, Herlitz L, Mohan C, Putterman C. Novel biomarker discovery through comprehensive proteomic analysis of lupus mouse serum. J Autoimmun. 2024;142:103134.
33. Gao HX, Sanders E, Tieng AT, Putterman C. Sex and autoantibody titers determine the development of neuropsychiatric manifestations in lupus-prone mice. J Neuroimmunol. 2010;229(1–2):112–22.
34. Moore E, Huang MW, Reynolds CA, Macian F, Putterman C. Choroid Plexus-infiltrating T cells as drivers of murine neuropsychiatric lupus. Arthritis Rheumatol. 2022;74(11):1796–807.
35. Herbert J, Wilcox JN, Pham KT, Fremeau RT Jr., Zeviani M, Dwork A, et al. Transthyretin: a choroid plexus-specific transport protein in human brain. The 1986 S. Weir Mitchell award. Neurology. 1986;36(7):900–11.
36. Bardenbacher M, Ruder B, Britzen-Laurent N, Schmid B, Waldner M, Naschberger E, et al. Permeability analyses and three dimensional imaging of interferon gamma-induced barrier disintegration in intestinal organoids. Stem Cell Res. 2019;35:101383.
37. Rueden CT, Schindelin J, Hiner MC, DeZonia BE, Walter AE, Arena ET, et al. ImageJ2: ImageJ for the next generation of scientific image data. BMC Bioinformatics. 2017;18(1):529.
38. Muradashvili N, Tyagi R, Lominadze D. A dual-tracer method for differentiating transendothelial transport from paracellular leakage in vivo and in vitro. Front Physiol. 2012;3:166.
39. Araie M, Maurice D. The rate of diffusion of fluorophores through the corneal epithelium and stroma. Exp Eye Res. 1987;44(1):73–87.
40. Pile KD, Graham GG. Methotrexate. In: Parnham MJ, editor. Compendium of Inflammatory diseases. Basel: Springer Basel; 2016. pp. 934–42.
41. Au - Bardenbacher M, Au - Ruder B, Au - Britzen-Laurent N, Au - Naschberger E et al. Au - Becker C, Au - Palmisano R,. Investigating Intestinal Barrier Breakdown in Living Organoids. JoVE. 2020(157):e60546.
42. Piconese S, Gri G, Tripodo C, Musio S, Gorzanelli A, Frossi B, et al. Mast cells counteract regulatory T-cell suppression through interleukin-6 and OX40/OX40L axis toward Th17-cell differentiation. Blood. 2009;114(13):2639–48.
43. Danielsen EM, Hansen GH. Probing paracellular -versus transcellular tissue barrier permeability using a gut mucosal explant culture system. Tissue Barriers. 2019;7(1):1601955.
44. Warren RB, Smith RL, Campalani E, Eyre S, Smith CH, Barker JNWN, et al. Genetic variation in Efflux Transporters Influences Outcome to Methotrexate Therapy in patients with psoriasis. J Invest Dermatology. 2008;128(8):1925–9.
45. Wu T, Sheng Y, Qin YY, Kong WM, Jin MM, Yang HY, et al. Bile duct ligation causes opposite impacts on the expression and function of BCRP and P-gp in rat brain partly via affecting membrane expression of ezrin/radixin/moesin proteins. Acta Pharmacol Sin. 2021;42(11):1942–50.
46. Chen X, Unadkat JD, Mao Q. Tetrahydrocannabinol and its major metabolites are not (or are poor) substrates or inhibitors of human P-Glycoprotein [ATP-Binding Cassette (ABC) B1] and breast Cancer resistance protein (ABCG2). Drug Metab Dispos. 2021;49(10):910–8.
47. Morris ME, Rodriguez-Cruz V, Felmlee MA, SLC, Transporters ABC. Expression, localization, and species differences at the blood-brain and the blood-cerebrospinal fluid barriers. Aaps j. 2017;19(5):1317–31.
48. Le Vee M, Lecureur V, Stieger B, Fardel O. Regulation of drug transporter expression in human hepatocytes exposed to the proinflammatory cytokines tumor necrosis factor-alpha or interleukin-6. Drug Metab Dispos. 2009;37(3):685–93.
49. Sangha V, Hoque MT, Henderson JT, Bendayan R. Novel localization of folate transport systems in the murine central nervous system. Fluids Barriers CNS. 2022;19(1):92.
50. Cowan DS, Tannock IF. Factors that influence the penetration of methotrexate through solid tissue. Int J Cancer. 2001;91(1):120–5.
51. Henderson GB, Strauss BP. Characteristics of a novel transport system for folate compounds in wild-type and methotrexate-resistant L1210 cells. Cancer Res. 1990;50(6):1709–14.
52. Nigam SK, Bush KT, Martovetsky G, Ahn SY, Liu HC, Richard E, et al. The organic anion transporter (OAT) family: a systems biology perspective. Physiol Rev. 2015;95(1):83–123.
53. Geisler M, Hegedűs T. A twist in the ABC: regulation of ABC transporter trafficking and transport by FK506-binding proteins. FEBS Lett. 2020;594(23):3986–4000.

54. Stolarczyk EI, Reiling CJ, Paumi CM. Regulation of ABC transporter function via phosphorylation by protein kinases. Curr Pharm Biotechnol. 2011;12(4):621–35.
55. Crawford RR, Potukuchi PK, Schuetz EG, Schuetz JD. Beyond competitive inhibition: regulation of ABC transporters by Kinases and Protein-Protein Interactions as potential mechanisms of drug-drug interactions. Drug Metab Dispos. 2018;46(5):567–80.
56. Yu X, Kennedy RH, Liu SJ. JAK2/STAT3, not ERK1/2, mediates interleukin-6-induced activation of inducible nitric-oxide synthase and decrease in contractility of adult ventricular myocytes. J Biol Chem. 2003;278(18):16304–9.
57. Wegiel B, Bjartell A, Culig Z, Persson JL. Interleukin-6 activates PI3K/Akt pathway and regulates cyclin A1 to promote prostate cancer cell survival. Int J Cancer. 2008;122(7):1521–9.
58. Nishikai-Yan Shen T, Kanazawa S, Kado M, Okada K, Luo L, Hayashi A, et al. Interleukin-6 stimulates akt and p38 MAPK phosphorylation and fibroblast migration in non-diabetic but not diabetic mice. PLoS ONE. 2017;12(5):e0178232.
59. Tang B, Matsuda T, Akira S, Nagata N, Ikehara S, Hirano T, et al. Age-associated increase in interleukin 6 in MRL/lpr mice. Int Immunol. 1991;3(3):273–8.
60. Vulsteke C, Lambrechts D, Dieudonné A, Hatse S, Brouwers B, van Brussel T, et al. Genetic variability in the multidrug resistance associated protein-1 (ABCC1/MRP1) predicts hematological toxicity in breast cancer patients receiving (neo-)adjuvant chemotherapy with 5-fluorouracil, epirubicin and cyclophosphamide (FEC). Ann Oncol. 2013;24(6):1513–25.
61. Yamamura M, Hanamura K, Koganezawa N, Furubayashi S, Shirao T, Kawabe H. Impacts of methotrexate on survival, dendrite development, and synapse formation of cortical neurons. Genes Cells. 2023;28(8):563–72.
62. Bhojwani D, Sabin ND, Pei D, Yang JJ, Khan RB, Panetta JC, et al. Methotrexate-induced neurotoxicity and leukoencephalopathy in childhood acute lymphoblastic leukemia. J Clin Oncol. 2014;32(9):949–59.
63. Jang A, Petrova B, Cheong TC, Zawadzki ME, Jones JK, Culhane AJ, et al. Choroid plexus-CSF-targeted antioxidant therapy protects the brain from toxicity of cancer chemotherapy. Neuron. 2022;110(20):3288–e3018.
64. Ibrahim KM, Darwish SF, Mantawy EM, El-Demerdash E. Molecular mechanisms underlying cyclophosphamide-induced cognitive impairment and strategies for neuroprotection in preclinical models. Mol Cell Biochem. 2023.
65. Robbiani DF, Finch RA, Jäger D, Muller WA, Sartorelli AC, Randolph GJ. The leukotriene C(4) transporter MRP1 regulates CCL19 (MIP-3beta, ELC)-dependent mobilization of dendritic cells to lymph nodes. Cell. 2000;103(5):757–68.
66. Fang SH, Wei EQ, Zhou Y, Wang ML, Zhang WP, Yu GL, et al. Increased expression of cysteinyl leukotriene receptor-1 in the brain mediates neuronal damage and astrogliosis after focal cerebral ischemia in rats. Neuroscience. 2006;140(3):969–79.
67. Kang KH, Liou HH, Hour MJ, Liou HC, Fu WM. Protection of dopaminergic neurons by 5-lipoxygenase inhibitor. Neuropharmacology. 2013;73:380–7.
68. Michael J, Unger MS, Poupardin R, Schernthaner P, Mrowetz H, Attems J, et al. Microglia depletion diminishes key elements of the leukotriene pathway in the brain of Alzheimer's disease mice. Acta Neuropathol Commun. 2020;8(1):129.
69. Attaluri S, Upadhya R, Kodali M, Madhu LN, Upadhya D, Shuai B, et al. Brain-specific increase in Leukotriene Signaling accompanies chronic neuroinflammation and cognitive impairment in a model of Gulf War Illness. Front Immunol. 2022;13:853000.
70. Riopelle RJ, Kennedy JC. Some aspects of porphyrin neurotoxicity in vitro. Can J Physiol Pharmacol. 1982;60(5):707–14.
71. Gerischer LM, Scheibe F, Nümann A, Köhnlein M, Stölzel U, Meisel A. Acute porphyrias - a neurological perspective. Brain Behav. 2021;11(11):e2389.
72. Trysberg E, Nylen K, Rosengren LE, Tarkowski A. Neuronal and astrocytic damage in systemic lupus erythematosus patients with central nervous system involvement. Arthritis Rheum. 2003;48(10):2881–7.
73. Han X, Xu T, Ding C, Wang D, Yao G, Chen H, et al. Neuronal NR4A1 deficiency drives complement-coordinated synaptic stripping by microglia in a mouse model of lupus. Signal Transduct Target Ther. 2022;7(1):50.
74. Ercan E, Magro-Checa C, Valabregue R, Branzoli F, Wood ET, Steup-Beekman GM, et al. Glial and axonal changes in systemic lupus erythematosus measured with diffusion of intracellular metabolites. Brain. 2016;139(5):1447–57.
75. Sarbu MI, Sarbu N. Fulminant brain atrophy and Vasculitis on Vessel-Wall Imaging in Neuropsychiatric Lupus: Case Report and Literature Review. Arch Rheumatol. 2020;35(3):443–8.
76. Dani N, Herbst RH, McCabe C, Green GS, Kaiser K, Head JP, et al. A cellular and spatial map of the choroid plexus across brain ventricles and ages. Cell. 2021;184(11):3056–e7421.
77. Saunders NR, Dziegielewska KM, Fame RM, Lehtinen MK, Liddelow SA. The choroid plexus: a missing link in our understanding of brain development and function. Physiol Rev. 2023;103(1):919–56.

Publisher's note